RILEM Technical Letters (2022) 7: 189-198
https://doi.org/10.21809/rilemtechlett.2022.166

Methods of incorporation of new reaction products in thermodynamic databases of cementitious systems

Tongren Zhu[1], Maria Juenger[1], O. Burkan Isgor[2], Lynn E. Katz[1]*

[1] University of Texas at Austin; Department of Civil, Architectural and Environmental Engineering; 301 E. Dean Keeton St. C1700, Austin, TX 78712, USA
[2] Oregon State University; Civil and Construction Engineering, Corvallis, OR 97331, USA

Received: 22 July 2022 / Accepted: 18 December 2022 / Published online: 31 January 2023

Abstract

Strategic blending of supplementary cementitious materials (SCMs) into ordinary portland cement (OPC) helps reduce energy use and greenhouse gas emissions from concrete production. Expanding thermodynamic databases to include new reaction products from blended cements improves computational approaches used to understand the impact of blending SCMs with cement. Determination of thermodynamic parameters of cement reaction products based on temperature-dependent solubility is widely used in cement research; however, assumptions, limitations, and potential errors due to intercorrelation of the thermodynamic parameters in these calculation methods are rarely discussed. Here, methods for obtaining thermodynamic parameters are critically reviewed, including discussion of experimental validation. The discussion herein provides useful guidance to improve and validate the process of determining thermodynamic parameters of new reaction products from SCM-OPC reactions.

Keywords: Cement reaction products; Thermodynamic models; Solubility

1 Introduction

Portland cement is the most energy intensive ingredient in concrete, the most widely used building material and second most manufactured product after potable water [1]. The production of portland cement accounts for approximately 5-8% of global carbon dioxide emissions [2]. The concrete industry has been striving toward reducing these impacts through various approaches. For example, strategic blending of supplementary cementitious materials (SCMs) into ordinary portland cement (OPC) helps reduce energy use and greenhouse gas emissions from concrete production [3,4]. The ability to predict the reactions of cementitious materials in concrete helps optimize mixtures for different performance criteria including durability and carbon footprint [5,6]. Thermodynamic modeling allows the prediction of hydrated cement phase assemblages and chemical compositions for a variety of cementitious material combinations [7–9]. Therefore, thermodynamic modeling can provide a computational approach to facilitate understanding of the impact of blending SCMs or other materials with cement on the chemical composition of the hydrated cementitious mixture.

Accurate thermodynamic modeling of cementitious systems relies on accurate and complete thermodynamic databases that include all possible reactants and products of the cement reactions [10]. CEMDATA, developed by the Swiss Federal Laboratories for Materials Testing and Research (EMPA), is the most widely used cement database and covers a large range of compounds that form in reactions of cementitious systems including OPC, SCMs and other binders. The latest version, CEMDATA18, is written in formats supporting both Gibbs Energy Minimization-Selector (GEMS) and PHREEQC, two thermodynamic modeling frameworks that use different approaches for modeling chemical systems [10–12]. GEMS simulates phase assemblages of the reaction products by minimizing the total Gibbs free energy of the system [12]. PHREEQC, on the other hand, is based on the law of mass action (LMA) and performs simulations by iteratively solving a system of mole balance and charge balance equations [11]. The LMA-based thermodynamic models are most commonly used in reactive transport models to calculate equilibrium speciation due to the simplicity of the algorithm [13,14]. However, since the LMA solvers have limitations when multicomponent phases (e.g., solid solutions, non-ideal liquids, and gaseous phases) are considered, the Gibbs energy minimization algorithm is generally the method of choice for simulations of complex multiphase systems [12]. As a result, cementitious systems have been traditionally modeled using GEMS, although the use of LMA-based codes, specifically PHREEQC, has been increasing for modeling cementitious systems [15]. Both GEMS and PHREEQC frameworks can be used to solve for concentrations of chemical species, their activity coefficients, chemical potentials of chemical

*Corresponding author: Lynn E. Katz, E-mail: lynnkatz@mail.utexas.edu

elements, and other thermodynamic quantities such as pH, fugacities, and the redox state of the system (i.e., pe). One major advantage of GEMS is its ability to calculate volume fractions of solid reaction products, as well as liquid and gas phases, so that estimates of capillary porosity and chemical shrinkage can be obtained.

The major limitation associated with modeling blended cement is the lack of thermodynamic data for the new solid reaction products that do not exist in the current thermodynamic databases; stoichiometry, solubility data, and thermodynamic constants required to predict temperature effects and porosity have not been determined or included in the CEMDATA database. These data need to be determined, and the compounds need to be added to the CEMDATA database to extend the application of thermodynamic modeling of reactions in cementitious systems. Because the GEMS version of the database can be converted to the PHREEQC database [10], this paper focuses on incorporating thermodynamic data into a database for GEMS use. In a Gibbs free energy minimization model (e.g., GEMS), the overall reaction is independent of the form of the input species but depends on the stoichiometric composition of the elements in the input recipe. In GEMS, the input recipe for complex cementitious systems such as SCMs (e.g. fly ash, pumice, etc.) is usually entered in the form of total molar (or mass) concentration of each component (typically in the form of oxides) determined from chemical analysis (e.g., x-ray fluorescence (XRF)) rather than distinct chemical compounds. As long as the correct molar (or mass) inputs of elements of all the reactants are available, stoichiometry is able to describe every species in the reaction products [12]. Therefore, application of GEMS is only limited by the availability of thermodynamic parameters for new solid reaction products [16].

This paper aims to provide a brief overview of the required thermodynamic parameters in the CEMDATA database and the experimental and mathematical methods used to obtain the parameters. Several mathematical methods to obtain thermodynamic parameters based on experimentally-determined solubility data are critically analyzed and compared. It should be noted that the methods used to determine the thermodynamic data that are necessary for adding a reaction product to CEMDATA depend on whether the chemical processes/reactions that lead to the formation of that compound are known. In cementitious systems, however, it can be difficult to know (or even hypothesize) these chemical reactions in many cases. As a result, many assumptions might be necessary to complete the thermodynamic data; in many cases, these data might be inter-dependent, expanding the errors originating in one parameter to others. Discussion in this paper assumes that reactions that lead to the formation of the product that is being added to the CEMDATA database are known, or at the very least, can be estimated because the chemical form of the product resembles another species that is already in the CEMDATA database.

2 Thermodynamic data

Table 1 lists the thermodynamic parameters required to incorporate a new solid reaction product into the CEMDATA database for GEMS. Since GEMS performs simulations of cementitious reactions by minimizing the Gibbs free energy of the end-members, the standard molar Gibbs free energy of formation of the new solid reaction product is needed. The Gibbs free energy of a reaction can be calculated from the measured solubility constant for the dissolution reaction of a solid phase:

$$\Delta_r G_T^0 = -RTlnK_T \quad (1)$$

where R is the universal gas constant (8.314 J/K/mol/) and K_T is the equilibrium solubility product at temperature *T (K)*. Therefore, experimental determination of the solubility constant from dissolution (or precipitation) of a solid reaction product is typically performed to calculate the Gibbs free energy associated with the reaction. The standard thermodynamic parameters at 25 °C and 1 bar are used for entry into the CEMDATA database [10]. During the simulation, the GEMS software performs temperature and pressure corrections using the Helgeson-Kirkham-Flowers equation [17]. The Gibbs free energy of a solid phase at a specific temperature is calculated from the Gibbs free energy at standard conditions as:

$$\Delta_f G_T^0 = \Delta_f G_{T_0}^0 - (T - T_0)S_{T_0}^0 - \int_{T_0}^{T}\int_{T_0}^{T}\frac{C_p^0}{T}dTdT \quad (2)$$

As a result, values for the standard molar entropy $S_{T_0}^0$, enthalpy $\Delta_f H_{T_0}^0$ and heat capacity $C_{p,T}^0$ of the solid phase are also needed. The heat capacity at constant pressure is calculated by:

$$C_{p,T}^0 = a_0 + a_1 T + a_2 T^{-2} + a_3 T^{-0.5} \quad (3)$$

where a_0, a_1, a_2, and a_3 are empirical heat capacity parameters. Molar volume of the solid reaction product is needed because GEMS also predicts the volume of each reaction product. The molar volume at standard conditions is also needed for the pressure correction of condensed substances (e.g., solids) if the simulation pressure is different from the standard state condition [18]. The approach to obtain each thermodynamic parameter is discussed in the subsequent sections.

Table 1. List of required thermodynamic parameters of new solid reaction product.

Thermodynamic Parameter	Unit	Definition
$logK_{S0}$	n/a	Logarithm of solubility constant at standard condition
$\Delta_f G^0_{T_0}$	kJ/mol	Standard molar Gibbs free energy of formation at standard condition
$\Delta_f H^0_{T_0}$	kJ/mol	Standard molar enthalpy of formation at standard condition
$S^0_{T_0}$	J/K/mol	Standard molar absolute entropy at standard condition
a_0	J/K/mol	Empirical heat capacity parameter
a_1	J/K^2/mol	Empirical heat capacity parameter
a_2	J·K/mol	Empirical heat capacity parameter
a_3	J/K$^{0.5}$/mol	Empirical heat capacity parameter
V^0	cm^3/mol	Molar volume at standard condition

2.1 Solubility constant

Solubility of a new solid reaction product is experimentally determined at various temperatures within the relevant temperature range of the cementitious reactions [19–21]. Suppose the composition of the new solid phase is $Ca_iAl_jSi_kO_l \cdot mH_2O$ and its dissolution reaction proceeds as Eq. 4:

$$Ca_iAl_jSi_kO_l \cdot mH_2O \rightarrow iCa^{2+} + jAlO_2{}^- + kSiO_2{}^0 + mH_2O \quad (4)$$

The composition of the new solid reaction product can be determined by quantifying the component concentrations (i.e., ionic oxides composition) and bound water content of the solid. The components in the form of ionic oxides are generally determined by XRF as the mass percentage of each oxide in the sample [22,23]. The components can also be determined by a combination of inductively coupled plasma-optical emission spectroscopy (ICP-OES) to obtain major element concentrations, ICP-Mass Spectroscopy (ICP-MS) to obtain minor element concentrations, and ion chromatography (IC) to obtain anion concentrations after digestion of the sample [24–28]. Digestion converts solids into liquid extracts to determine the metal or anion content. The digestion solution can be a combination of acids (e.g., nitric acid, hydrochloric acid, hydrofluoric acid) and peroxide per standard methods [29–31] or proprietary digestion solutions depending on the type of solid [24]. Typically, microwave radiation is used to accelerate the digestion process [30,31]. After determination of the components in the solid, the oxygen content of the solid is quantified via stoichiometry of the corresponding oxide.

Bound water content of the solids can be determined by thermogravimetric analysis (TGA) under N_2. The amount of bound water is calculated from the mass loss of the sample between 105°C and 1000 °C as recommended by RILEM TC 238-SCM [32]. However, one should be cautious about the assumption that all evaporable water is removed at 105 °C. Some studies found evaporable water at temperatures up to 130 °C [33]; these researchers recorded bound water mass loss starting from 145-150 °C instead of 105 °C [34,35]. On the other hand, loss of chemically bound water from C-S-H, AFm, and ettringite below 105 °C has been reported [36–39]. To remove evaporable water without inducing loss of structural water below 105 °C, some studies vacuum-filtered and equilibrated the sample at a lower temperature (e.g., 40 °C) for an hour under N_2 to allow the evaporation of excess water [24]. Freeze-drying has also been proposed as a suitable procedure; however it can still cause some change to the microstructure, therefore it is preferred over oven drying [36,40,41]. Mass loss at higher temperatures can occur due to decarbonation, which occurs at 600-800 °C [42,43]. To avoid interferences in bound water measurements from decarbonation, some studies limited their TGA upper range temperatures to 500-600 °C [19,24,44]. However, whether an upper temperature lower than 1000 °C would underestimate the content of bound water is not discussed in these studies, possibly because the impact of higher temperatures on bound water content is expected to be minimal.

The solubility of a new solid (e.g. $Ca_iAl_jSi_kO_l \cdot mH_2O$) is experimentally determined from either dissolution or precipitation. In the dissolution approach, the synthesized dry solid is dispersed in degassed water (by boiling) and stored in plastic bottles (HDPE or PTFE) [19,20,24]. The sealed bottles are then kept in suspension isothermally at several selected temperature points until the dissolution reaction reaches equilibrium as determined from statistically constant measurements of reaction products from sample aliquots measured over time [19,45,46]. The time for the dissolution reaction to reach equilibrium can vary with respect to the solid phase, temperature and solution conditions. ICP-OES is often used for analysis of major dissolution products such as Si, Al, Ca. Researchers should prepare standard sets with a matrix close to the supernatant samples from the highly saline system to ensure that the matrix effect is accounted for [24].

In the precipitation approach, reacting solutions prepared using deionized, degassed water are mixed in plastic bottles to form the new solid reaction product [20,24]. CO_2 will significantly interfere with cement reactions in alkaline conditions; therefore, the solution preparation, transferring, and mixing should be performed in a N_2-filled glove box [19,20,24,47]. The time for the precipitation reaction to reach equilibrium can again be determined by sampling supernatant aliquots for reactant analysis over time [24]. Once the measured aqueous concentration of metals remains stable over several (3-5) sampling events, equilibrium is assumed. However, in some cases amorphous phases can be stable for a period of time and the length of the sampling period should be sufficient to ensure that a crystalline phase has formed [48]; X-ray diffraction (XRD) can be useful in this regard.

After equilibrium has been obtained, the solutions are filtered through a membrane filter and acidified with HNO_3. The aqueous metal content is determined by ICP-OES or ICP-MS. The type of membrane used for filtration is selected to ensure minimal adsorption of dissolved metals onto the membrane and successful capture of solids. The type and pore size of the membranes are seldom discussed in literature; however, it has been reported that measured solubility of minerals filtered through a 3kD membrane is much lower than that filtered through a 0.05 µm membrane [49]. Considering most membrane filters used in cement systems for solid-liquid separation are 0.22 or 0.45 µm in pore size [20,47,50,51], it is possible that some fraction of small undissolved solids will pass the membrane to be measured as dissolution products. Therefore, in addition to using membranes with smaller pore size where possible, it is necessary to experimentally characterize (e.g., using nanoparticle tracking analysis) the filtrate after membrane filtration to ensure minimum presence of solids.

The measured aqueous metal content is then used together with speciation modeling to calculate the concentration of aqueous species to yield the solubility constant via Eq. 5:

$$K_{S0} = \{Ca^{2+}\}^i \cdot \{AlO_2^-\}^j \cdot \{SiO_2^0\}^k \cdot \{H_2O\}^m = (\gamma_i[Ca^{2+}])^i \cdot (\gamma_j[AlO_2^-])^j \cdot (\gamma_k[SiO_2^0])^k \cdot (\gamma_{H_2O}[H_2O])^m \quad (5)$$

where γ_i is the corresponding activity coefficient of the dissolved aqueous species. Activity coefficients of the relevant species can be calculated by various models. The Davies equation is generally valid for ionic strengths between 0.1 to 0.7 M [52]. The specific ion interaction theory (SIT) model is generally applicable up to 3-4 M [53]. At an even higher ionic strength, a more complex model such as the Pitzer ion-interaction model is required [54]. In the application of cementitious reactions, the Helgeson modification of the Truesdell-Jones version of the extended Debye-Huckel Equation (Eq. 6) is often used and is applicable to ionic strengths up to 1-2M [52,55]:

$$log\gamma_i = \frac{-Az_i^2\sqrt{I}}{1+Ba\sqrt{I}} + bI \quad (6)$$

In Eq. 6, γ_i is the activity coefficient of ion I, A and B are Debye-Huckel solvent parameters, z_i is the ionic charge, I is the ionic strength of the solution, a is a parameter dependent on the size of the parameter, and b is a semi-empirical parameter. In most cementitious applications, Eq. 6 has only considered a and b for the major background electrolyte (NaOH, KOH, NaCl, and KCl) [55].

While the Pitzer model is seldom used for cementitious systems, it is probably the most applicable model for alkali-activated reactions of SCMs where highly alkaline solutions (e.g., > 4 M NaOH) are generally used as the activating solution (i.e., geopolymers) [56–61]. However, the Pitzer model requires specific ion interaction parameters, which may not be available for cementitious compositions.[62] Moreover, the Piter model is not directly incorporated into GEM-Selektor, the most common geochemical software for modeling cementitious systems [62–64]. As a result, Eq. 6 is still widely used for alkali-activated reactions despite it being only applicable to 1-2 M [63,65,66].

2.2 Heat capacity

As shown in Eq. 2, heat capacity is needed to calculate Gibbs free energy at a temperature different from the standard state condition (i.e., 25 °C). The heat capacity of a solid can be calculated via Eq. 3. While a few studies measured heat capacity experimentally using thermal relaxation calorimetry and differential scanning calorimetry (DSC) [67,68], in the field of cement research, the heat capacity is usually estimated using a reference reaction [20,69] or via the additive approach of elementary oxides [47,70]. The reference reaction approach adopts heat capacity values for solids with known heat capacity that are structurally similar to the new solid reaction product of interest [20,69]. For example, if the unknown new solid A is structurally similar to the aluminate ferrite monosulfate (AFm) family, the reference reaction could include a known AFm [20,50,71]. A few examples are shown in Table 2.

Because heat capacity differs greatly between free water and structurally-bound water, the reference reaction only involves solids without free water, thus the change in heat capacity of the reference reaction is approximately zero. For example, if the new solid reaction product A can be written into a reference reaction, Eq. 7:

$$A + bB \rightarrow cC + dD \quad (7)$$

where B, C, and D are species with known values of heat capacity parameters, the empirical heat capacity parameters a_i of solid A can be estimated using Eq. 8:

$$a_{i,A} = c \cdot a_{i,C} + d \cdot a_{i,D} - b \cdot a_{i,B} \quad (8)$$

The values of heat capacity parameters of the known species B, C, and D can be found from the built-in Nagra-PSI thermodynamic database in GEMS, the existing CEMDATA18 database, or published literature [72,73].

Table 2. Reference reactions used to calculate heat capacity based on structurally similar phases.

Unknown phases	Type	Reference Reaction	Reference
$Ca_4Al_2(OH)_{14}{\cdot}6H_2O$	Hydroxy-AFm	$Ca_4Al_2(OH)_{14}{\cdot}6H_2O + CaSO_4 \rightarrow Ca_4Al_2SO_4(OH)_{12}{\cdot}6H_2O + Ca(OH)_2$	[20]
$Ca_4Al_2(SO_4)_{0.5}(Cl)\ (OH)_{12}{\cdot}6H_2O$	Cl-AFm	$Ca_4Al_2(SO_4)_{0.5}(Cl)\ (OH)_{12}{\cdot}6H_2O + 0.5\ CaSO_4 \rightarrow Ca_4Al_2SO_4(OH)_{12}{\cdot}6H_2O + 0.5CaCl_2$	[71]

In the additive elementary oxides approach, the heat capacity of a solid phase whose composition is $Ca_iAl_jSi_kO_l \cdot mH_2O$ can be treated as the stoichiometric addition of heat capacity of CaO, Al_2O_3, SiO_2, and zeolitic H_2O:

$$C^0_{p,Ca_iAl_jSi_kO_l \cdot mH_2O} = \sum \nu_i C_{p,i} \quad (9)$$

where ν_i represents the stoichiometric number, and $C_{p,i}$ is the heat capacity of the ith elementary component. Heat capacity at different temperatures can also be obtained by addition of heat capacities of elementary oxides at different temperatures with their stoichiometry. The temperature-heat capacity relationship obtained can be fitted to Eq. 3 to obtain the empirical heat capacity parameters a_i.

2.3 Standard molar enthalpy, entropy, and Gibbs free energy

Several methods have been used to obtain enthalpy, entropy and Gibbs free energy of formation of the solid phase depending on the level of assumptions employed.

The van't Hoff model assumes constant enthalpy of the dissolution reaction (e.g., Eq. 4) and fits the log of the solubility products at different temperature as Eq. 10. An example of using the van't Hoff model to fit solubility data of crystalline sodium aluminosilicate (N-A-S-(H)) is shown in Figure 1a [74].

$$logK_T = \frac{0.4343}{R}\left(\Delta_r S^0_{T_0} - \frac{\Delta_r H^0_{T_0}}{T}\right) \quad (10)$$

By fitting Eq. 10, enthalpy and entropy of the dissolution reaction can be obtained. The obtained $\Delta_r S^0_{T_0}$ and $\Delta_r H^0_{T_0}$ can be used to yield the Gibbs free energy of the reaction as shown in Eq. 11:

$$\Delta_r G^0_{T_0} = \Delta_r H^0_{T_0} - T_0 \Delta_r S^0_{T_0} \quad (11)$$

The standard Gibbs free energy of formation, $\Delta_f G^0_{T_0}$ for the phase is then obtained using Eq. 12 if the known thermodynamic parameters of reactants and products are available. In the example of a dissolution reaction shown as Eq. 4, $\Delta_f G^0_{T_0}$ of $Ca_iAl_jSi_kO_l \cdot mH_2O$ can be calculated as:

$$\Delta_f G^0_{T_0} = i \cdot \Delta_f G^0_{T_0,Ca^{2+}} + j \cdot \Delta_f G^0_{T_0,AlO_2^-,} + k \cdot \Delta_f G^0_{T_0,SiO_2{}^0} + m \cdot \Delta_f G^0_{T_0,H_2O} - \Delta_r G^0_{T_0} \quad (12)$$

Similarly, the standard molar enthalpy and entropy of $Ca_iAl_jSi_kO_l \cdot mH_2O$ are calculated using the known standard state properties of the aqueous species:

$$\Delta_f H^0_{T_0} = i \cdot \Delta_f H^0_{T_0,Ca^{2+}} + j \cdot \Delta_f H^0_{T_0,AlO_2^-,} + k \cdot \Delta_f H^0_{T_0,SiO_2{}^0} + m \cdot \Delta_f H^0_{T_0,H_2O} - \Delta_r H^0_{T_0} \quad (13)$$

$$S^0_{T_0} = i \cdot S^0_{T_0,Ca^{2+}} + j \cdot S^0_{T_0,AlO_2^-,} + k \cdot S^0_{T_0,SiO_2{}^0} + m \cdot S^0_{T_0,H_2O} - \Delta_r S^0_{T_0} \quad (14)$$

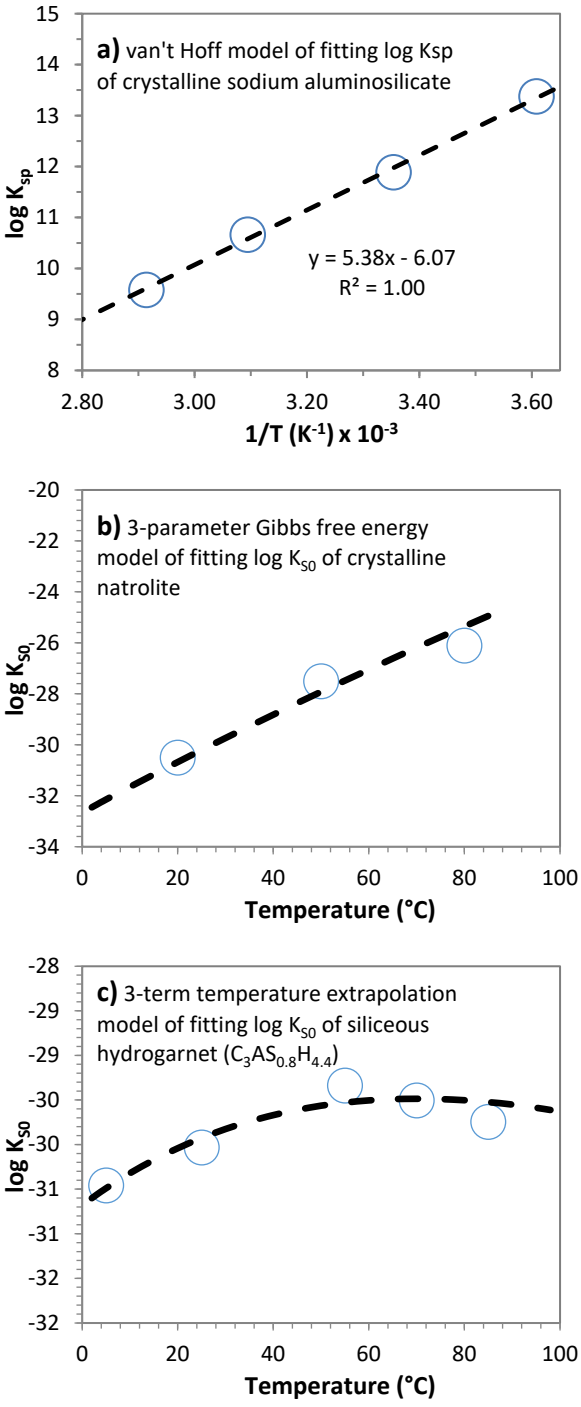

Figure 1. a) van't Hoff model of fitting solubility data of crystalline N-A-S-(H) (from Williamson *et al.,* 2022) [74]; b) 3-parameter Gibbs free energy model of fitting solubility data of natrolite (from *Lothenbach et al.,* 2017) [47]; and c) 3-term temperature extrapolation method of fitting solubility data of siliceous hydrogarnet (from Matschei *et al.*, 2007) [20].

The three-parameter Gibbs free energy model fits calculated Gibbs free energy of formation values of the phase at different temperature according to Eq. 1 and 2 [47,70,75]. The experimentally-determined solubility products of the dissolution reaction, K_T, at different temperature points can be used to calculate the Gibbs free energy of the dissolution

reaction, $\Delta_r G_T^0$, at different temperatures. For the dissolution reaction shown in Eq. 4, the $\Delta_f G_T^0$ of the new solid phase at different temperatures can be obtained in a similar manner as employed for Eq. 12 if $\Delta_f G_T^0$ of each aqueous species is known for a range of temperatures.

The heat capacity of the solid is assumed constant over the relevant temperature range; therefore, C_p^0 in Eq. 2 can be treated as a constant and the equation can be integrated and simplified to yield Eq. 15 [47,70,75]:

$$\Delta_f G_T^0 = \Delta_f G_{T_0}^0 - S_{T_0}^0(T - T_0) - C_p^0\left(T ln\frac{T}{T_0} - T + T_0\right) \quad (15)$$

The heat capacity, C_p^0, and entropy, $S_{T_0}^0$, of the new solid phase are typically estimated using the additivity method with the elementary oxide components [70,75,76]. This approach estimates C_p^0 using Eq. 9 and estimates $S_{T_0}^0$ using Eq. 16:

$$S_{T_0,Ca_iAl_jSi_kO_l\cdot mH_2O}^0 = \frac{\sum \nu_i S_{T_0,i}^0 (\sum \nu_i V_i^0 - V^0)}{2\sum \nu_i V_i^0} \quad (16)$$

where ν_i represents the stoichiometric number, $S_{T_0,i}^0$ is the standard molar entropy, and V_i^0 is the molar volume of the ith elementary components; V^0 is the molar volume of the new solid phase. While this approach is useful for crystalline phases, its use in estimating C_p^0 and $S_{T_0}^0$ for amorphous phases may be limited as C_p^0 and $S_{T_0}^0$ values of amorphous elementary oxides are generally not available.

The standard molar Gibbs free energy of formation, $\Delta_f G_{T_0}^0$ can be obtained by fitting the Gibbs free energies of formation for a range of temperatures using Eq. 15. An example of using the three-parameter Gibbs free energy model to fit the solubility data of natrolite is shown in Figure 1b [47].

The three-term temperature extrapolation model assumes the heat capacity of the dissolution reaction $\Delta_r Cp_T^0$ is constant over the relevant temperature range and fits the 3-term equation shown in Eq. 17 [77,78]:

$$logK_T = A_0 + A_2 T^{-1} + A_3 lnT \quad (17)$$

The relationship of thermodynamic parameters and the "$logK$" function shown in Eqs. 18 to 20 are then used to obtain the thermodynamic parameters of the dissolution reaction [8,20]:

$$A_0 = \frac{0.4343}{R}\left[\Delta_r S_{T_0}^0 - \Delta_r Cp_{T_0}^0(1 + lnT_0)\right] \quad (18)$$

$$A_2 = -\frac{0.4343}{R}\left(\Delta_r H_{T_0}^0 - \Delta_r Cp_{T_0}^0 T_0\right) \quad (19)$$

$$A_3 = \frac{0.4343}{R}\Delta_r Cp_{T_0}^0 T_0 \quad (20)$$

The molar entropy of the reaction, $\Delta_r S_{T_0}^0$, and the molar enthalpy of the reaction, $\Delta_r H_{T_0}^0$, are estimated from Eq. 18 and 19, respectively, by regression of the "$logK$" function in Eq. 17. The heat capacity of the reaction, $\Delta_r Cp_{T_0}^0 T_0$, is generally not fitted using Eq. 20; rather, it is estimated from reference reactions as discussed in section 2.2.[8,20] The Gibbs free energy of the reaction can be obtained from Eq. 11, and the standard Gibbs free energy of formation, $\Delta_f G_{T_0}^0$ for the new solid phase is then obtained using Eq. 12. The standard molar enthalpy of formation $\Delta_f H_{T_0}^0$ and entropy $S_{T_0}^0$ of the new solid phase $Ca_iAl_jSi_kO_l\cdot mH_2O$ are calculated using Eq. 13 and 14. An example of using the three-term temperature extrapolation model to fit the solubility data of siliceous hydrogarnet is shown in Figure 1c [20].

2.4 Molar volume

Molar volume of the new solid reaction product phase is needed so that the simulation can predict the volume fraction of the formed phases and thus porosity of the cementitious system. The molar volume V^0 is calculated by dividing the molecular weight MW by the density ρ of the solid phase as shown in Eq. 21:

$$V^0 = \frac{MW}{\rho} \quad (21)$$

One common technique to obtain the density of the new solid is gas pycnometry using helium gas [51,79–81]. This method measures the pressure change resulting from displacement of helium by the solid. After drying, the pre-weighed solid sample is placed into the pycnometer to obtain the density of the solid sample [51].

When the new solid of interest is crystalline, the density of the new solid can also be estimated from crystallographic data and unit cell constants determined by XRD [82,83]. However, if the cement reaction product of interest is amorphous, XRD techniques are of limited use to determine the density of such solids.

3 Discussion

The three-parameter Gibbs free energy model and the three-term temperature extrapolation model as described in Section 2 have been widely used to expand CEMDATA over the past few decades [8,20,47,50,69,84]. The van't Hoff model has been used in some recent studies. [45,74]. By limiting the needed experimental work for solubility measurements at different temperatures, these three methods provide a relatively straightforward framework to incorporate new reaction products into the CEMDATA database. Nevertheless, researchers need to be aware of some intrinsic assumptions of these methods with respect to obtaining molar enthalpy, entropy, and Gibbs free energy.

All three methods to obtain molar enthalpy, entropy, and Gibbs free energy are based on fitting experimentally-determined K_T values. Both the three-parameter Gibbs free energy model and the three-term temperature extrapolation method require estimation of the heat capacity. In the three-parameter model, while estimating heat capacity and entropy from elementary oxides yields satisfactory results for crystalline phases, such estimation cannot be performed when the phase of interest is amorphous, as heat capacity or

entropy values for amorphous elementary oxides are difficult to obtain. In the three-term extrapolation model, the estimated heat capacity based on Eq. 7 and 8 requires the minerals in the reference reaction to be structurally similar to the new solid to allow the heat capacity of the reference reaction $\Delta_r Cp_T^0$ to be approximately zero. However, previous research has not set forth a systematic method for selecting the reference reaction, the only guidance is that known components from structurally similar phases to the new solid should be used and the importance of selecting a reference reaction without free water has been highlighted.[20,71] This assumption that $\Delta_r Cp_T^0$ is zero for the reference reaction risks error in determination of the heat capacity if $\Delta_r Cp_T^0$ of the reference reaction is not zero. In addition, the three-term extrapolation fitting procedure for enthalpy and entropy employing Equations 17-20 is somewhat circular because Equations 18-20 include fitting the reaction heat capacity term.

The van't Hoff approach, on the other hand, assumes constant enthalpy of the dissolution reaction which may be applicable over a small temperature range where the change in heat capacity of the dissolution reaction is negligible. A demonstration of using the van't Hoff model and the three-parameter Gibbs free energy model is provided here and shows that the simpler van't Hoff approach is sufficient for the relevant temperature range of cement hydration [74]. In this example, crystalline N-A-S-(H) samples were synthesized using sodium silicate and sodium aluminate solutions across a range of bulk aqueous Si/Al ratios at different temperatures following the precipitation approach discussed in Section 2.1. Concentrations of sodium, aluminum, and silica in the supernatants were measured, activities were calculated using PHREEQC and solubility constants were calculated following the N-A-S-(H) dissolution reaction shown in Eq. 22 in a similar manner as Eq. 5.

$$NaAlSi_{1.06}O_{4.12} \cdot 1.72H_2O_{(S)} - 1.6H_2O_{(l)} + 4H^+_{(aq)} \leftrightarrow \mathrm{Na}^+_{(aq)} + Al^{3+*}_{(aq)} + 1.06H_4SiO^o_{4(aq)} \quad (22)$$

Both the van't Hoff model and the three-parameter Gibbs free energy model were used to calculate thermodynamic parameters as shown in Table 3. The van't Hoff expression yielded similar Gibbs free energy of formation data as the three-parameter Gibbs free energy model. Thus, the van't Hoff approach may obviate the need for estimating the heat capacity from elementary oxide addition or reference reactions over reasonably small temperature ranges. However, one limitation of using a small temperature range is that the regression is not very sensitive to the value of entropy [74].

Table 3. Thermodynamic parameters of crystalline N-A-S-(H) calculated from three-parameter Gibbs free energy model and van't Hoff model.

	Parameters of N-A-S-(H) phases			
	$\Delta_f H^0_{T_0}$ (kJ/mol)	$S^0_{T_0}$ (J/mol·K)	$\Delta_f G^0_{T_0}$ (kJ/mol)	c^0_{p,T_0} (J/mol·K)
three-parameter	-2657.1	208.2	-2443.9	203.2
van't Hoff	-2674.2	152.7	-2444.5	281.6

4 Recommendation

Calculation of thermodynamic parameters are based on regressions of K_T. To mitigate the error in K_T based on measured concentrations, determining K_T for at least 4 or 5 temperature points is recommended. Experimental validation of thermodynamic parameters that are currently fitted or calculated is also recommended as discussed next.

Heat capacity of dry powders can be experimentally determined by thermal relaxation calorimetry and DSC [67,68,85]. Recently, the physical property measurement system (PPMS), a commercially available automated relaxation calorimeter , has been used to determine the heat capacity of solids [86,87]. By heating a mass of new solid in the PPMS or DSC over a temperature range, the heat capacity of the new solid can be calculated as [88]:

$$C^0_{p,T} = \frac{M_{TH}}{m/MW} \quad (23)$$

where M_{TH} is the measured thermal mass (J/K), m is mass of the solid sample (g), and MW is the molecular weight of the solid of interest. Nevertheless, limited studies have employed calorimetry techniques to determine heat capacity of cementitious reaction products [67,85]. Most studies still estimate heat capacity based on the methods described in Section 2. It is recommended that when the pure phase composition of the reaction products is known and advanced calorimetry techniques are available for heat capacity measurements, experimentally determined heat capacities should be obtained and compared to values determined from a reference equation or addition of elementary oxides. Not only will the experimentally determined data improve the accuracy of the thermodynamic parameter estimates, but the data will also help to validate the other estimation methods.

When the enthalpy of the reaction needs to be experimentally determined, solution calorimetry is used [85,89,90]. In this technique, the new solid is dissolved in a suitable solvent (e.g., 5 N HCl) and the heat released or consumed is recorded. The measured heat from the acid dissolution is then used with known or measured heat release data from reference compounds to obtain $\Delta_f H^0_{T_0}$ of the new solid.[85] However, accuracy of measured $\Delta_r H^0_{T_0}$ values for the dissolution reaction can be impacted by the presence of impurities in the synthesized new solid [69]. Therefore, use of experimentally-determined enthalpy values should also be employed with caution.

To validate estimated entropy values from fitting or calculation, experimentally-determined entropy values can

be calculated from the measured heat capacity over a range of temperatures and under constant pressure as shown in Eq. 24 [91,92]. However, determination of entropy from heat capacity measurement is hardly used for cement reaction products [93].

$$\Delta S_T^0 = \Delta S_{T=0}^0 + \int_0^T \frac{C_{p,T}^0}{T} dT \quad (24)$$

5 Conclusion

In summary, thermodynamic modeling is a valuable tool in the study of cementitious reactions with new SCMs if used with an accurate and complete database. Expanding the current database to include more solid reaction products that arise with the use of new SCMs will be the focus of future efforts. Estimation of thermodynamic parameters based on measured solubility products at several temperatures is a well established approach and has been widely used in many studies to expand the CEMDATA database. Nevertheless, this widely used framework of methods involves assumptions that might need further improvement when being extended to new reaction products of cementitious reactions.

Acknowledgments

The authors thank Advanced Research Projects Agency–Energy (ARPA-E) Grant DE-AR0001143 and National Science Foundation (NSF) Award CMMI-1903457 for financial support of the study presented in this paper.

Authorship Statement (CRediT)

Tongren Zhu: Conceptualization, Investigation, Writing – original draft

Maria Juenger: Conceptualization, Writing – review and editing, Supervision, Funding acquisition

O. Burkan Isgor: Conceptualization, Writing – review and editing, Funding acquisition

Lynn Katz: Conceptualization, Writing – review and editing, Supervision, Funding acquisition

References

[1] A. Hasanbeigi, L. Price, E. Lin, Emerging energy-efficiency and CO 2 emission-reduction technologies for cement and concrete production: A technical review, Renewable and Sustainable Energy Reviews. 16 (2012) 6220-6238. https://doi.org/10.1016/j.rser.2012.07.019

[2] L. Barcelo, J. Kline, G. Walenta, E. Gartner, Cement and carbon emissions, Materials and Structures/Materiaux et Constructions. 47 (2014) 1055-1065. https://doi.org/10.1617/s11527-013-0114-5

[3] T.R. Naik, R. Kumar, Sustainable concrete with industrial and postconsumer by-product materials, in: Second International Conference on Sustainable Construction Materials and Technologies, Ancona, Italy, June 28-30, 2010, 2010.

[4] C. Meyer, The greening of the concrete industry, Cem Concr Compos. 31 (2009) 601-605. https://doi.org/10.1016/j.cemconcomp.2008.12.010

[5] K. Bharadwaj, R.M. Ghantous, F. Sahan, O.B. Isgor, W.J. Weiss, Predicting pore volume, compressive strength, pore connectivity, and formation factor in cementitious pastes containing fly ash, Cem Concr Compos. 122 (2021) 104113. https://doi.org/10.1016/j.cemconcomp.2021.104113

[6] K. Bharadwaj, O.B. Isgor, W.J. Weiss, K.S.T. Chopperla, A. Choudhary, G.D. Vasudevan, D. Glosser, J.H. Ideker, D. Trejo, A New Mixture Proportioning Method for Performance- Based Concrete, Materials Journal. 119 (2022) 207-220.

[7] B. Lothenbach, F. Winnefeld, Thermodynamic modelling of the hydration of Portland cement, Cem Concr Res. 36 (2006) 209-226. https://doi.org/10.1016/j.cemconres.2005.03.001

[8] D. Damidot, B. Lothenbach, D. Herfort, F.P. Glasser, Thermodynamics and cement science, Cem Concr Res. 41 (2011) 679-695. https://doi.org/10.1016/j.cemconres.2011.03.018

[9] B. Lothenbach, M. Zajac, Application of thermodynamic modelling to hydrated cements, Cem Concr Res. 123 (2019) 105779. https://doi.org/10.1016/j.cemconres.2019.105779

[10] B. Lothenbach, D.A. Kulik, T. Matschei, M. Balonis, L. Baquerizo, B. Dilnesa, G.D. Miron, R.J. Myers, Cemdata18: A chemical thermodynamic database for hydrated Portland cements and alkali-activated materials, Cem Concr Res. 115 (2019) 472-506. https://doi.org/10.1016/j.cemconres.2018.04.018

[11] D.L. Parkhurst, C.A.J. Appelo, Description of input and examples for PHREEQC version 3-A computer program for speciation, batch-reaction, one-dimensional transport, and inverse geochemical calculations: U.S. Geological Survey Techniques and Methods, book 6, chap. A43, 2013. https://doi.org/10.3133/tm6A43

[12] D. Kulik, U. Berner, E. Curti, Modelling Chemical Equilibrium Partitioning with the GEMS-PSI Code, Paul Scherrer Institut Scientific Report Volume IV, CH-5232 Villigen PSI (Switzerland), 2003.

[13] A.M.M. Leal, D.A. Kulik, W.R. Smith, M.O. Saar, An overview of computational methods for chemical equilibrium and kinetic calculations for geochemical and reactive transport modeling, in: Pure and Applied Chemistry, Walter de Gruyter GmbH, 2017: pp. 597-643. https://doi.org/10.1515/pac-2016-1107

[14] W.R. Smith, R.W. Missen, Chemical Reaction Equilibrium Analysis: Theory and Algorithms, John Wiley, New York, 1983.

[15] N. Holmes, M. Tyrer, R. West, A. Lowe, D. Kelliher, Using PHREEQC to model cement hydration, Constr Build Mater. 319 (2022). https://doi.org/10.1016/j.conbuildmat.2021.126129

[16] D.A. Kulik, T. Wagner, S. V. Dmytrieva, G. Kosakowski, F.F. Hingerl, K. V. Chudnenko, U.R. Berner, GEM-Selektor geochemical modeling package: Revised algorithm and GEMS3K numerical kernel for coupled simulation codes, Comput Geosci. 17 (2013) 1-24. https://doi.org/10.1007/s10596-012-9310-6

[17] D.A. Sverjensky, E.L. Shock, H.C. Helgeson, Prediction of the thermodynamic properties of aqueous metal complexes to 1000°C and 5 kb, Geochim Cosmochim Acta. 61 (1997) 1359-1412. https://doi.org/10.1016/S0016-7037(97)00009-4

[18] GEMS Development Team, GEMS3 Theory TD Calculations, (n.d.). http://gems.web.psi.ch/TDB/doc/html/theory_tdb.html (accessed June 4, 2020).

[19] B.Z. Dilnesa, B. Lothenbach, G. Renaudin, A. Wichser, D. Kulik, Synthesis and characterization of hydrogarnet Ca3(Al xFe1 - X)2(SiO4)y(OH) 4(3 - y), Cem Concr Res. 59 (2014) 96-111. https://doi.org/10.1016/j.cemconres.2014.02.001

[20] T. Matschei, B. Lothenbach, F.P. Glasser, Thermodynamic properties of Portland cement hydrates in the system CaO-Al2O3-SiO2-CaSO4-CaCO3-H2O, Cem Concr Res. 37 (2007) 1379-1410. https://doi.org/10.1016/j.cemconres.2007.06.002

[21] T. Schmidt, B. Lothenbach, M. Romer, K. Scrivener, D. Rentsch, R. Figi, A thermodynamic and experimental study of the conditions of thaumasite formation, Cem Concr Res. 38 (2008) 337-349. https://doi.org/10.1016/j.cemconres.2007.11.003

[22] P. Stutzman, A. Heckert, NIST TN-1816: Performance Criteria For an ASTM XRF Standard Test Method For Chemical Analysis of Hydraulic Cements: Inter-Laboratory Study on Cements A and B, 2013. https://doi.org/10.6028/NIST.TN.1816

[23] P. Wedding, B. Wheeler, Chemical Analysis of Portland Cement by Energy Dispersive X-Ray Fluorescence, Cement, Concrete and Aggregates. 5 (1983) 123. https://doi.org/10.1520/CCA10262J

[24] T. Williamson, J. Han, L. Katz, G. Sant, M. Juenger, Method for experimentally determining N-A-S-(H) solubility, RILEM Technical Letters. 3 (2019) 104-113. https://doi.org/10.21809/rilemtechlett.2018.63

[25] W. Devos, C. Moor, Determination of 14 trace element concentrations in two Dillinger Hüttenwerke Portland cement reference materials by sector field and quadrupole ICP-MS, J Anal At Spectrom. 17 (2002) 138-141. https://doi.org/10.1039/B107106H

[26] S.S. Potgieter, L. Marjanovic, A further method for chloride analysis of cement and cementitious materials - ICP-OES, Cem Concr Res. 37 (2007) 1172-1175. https://doi.org/10.1016/j.cemconres.2007.05.006

[27] U.R. Funteas, J.A. Wallace, F.W. Fochtman, A Comparative Analysis Of Mineral Trioxide Aggregate And Portland Cement, Australian Endodontic Journal. 29 (2003) 43-44. https://doi.org/10.1111/j.1747-4477.2003.tb00498.x
[28] Y.L. Wei, C.L. Cheng, Determination of total Cl in incinerator fly ashes utilized as cement raw materials, Constr Build Mater. 124 (2016) 544-549. https://doi.org/10.1016/j.conbuildmat.2016.07.132
[29] USEPA, "Method 3050B: Acid Digestion of Sediments, Sludges, and Soils," Revision 2, Washington, DC, 1996. https://www.epa.gov/sites/production/files/2015-06/documents/epa-3050b.pdf.
[30] USEPA, "Method 3051A (SW-846): Microwave Assisted Acid Digestion of Sediments, Sludges, and Oils," Revision 1, Washington, DC, 2007. https://www.epa.gov/sites/production/files/2015-12/documents/3051a.pdf.
[31] USEPA, "Method 3052 (SW-846): Microwave Assisted Acid Digestion of Siliceous and Organically Based Matrices," Revision 0, Washington, DC, 1996. https://www.epa.gov/sites/production/files/2015-12/documents/3052.pdf.
[32] K.L. Scrivener, B. Lothenbach, N. De Belie, E. Gruyaert, J. Skibsted, R. Snellings, A. Vollpracht, TC 238-SCM: hydration and microstructure of concrete with SCMs: State of the art on methods to determine degree of reaction of SCMs, Mater Struct. 48 (2015) 835-862. https://doi.org/10.1617/s11527-015-0527-4
[33] S. Kourounis, S. Tsivilis, P.E. Tsakiridis, G.D. Papadimitriou, Z. Tsibouki, Properties and hydration of blended cements with steelmaking slag, Cem Concr Res. 37 (2007) 815-822. https://doi.org/10.1016/j.cemconres.2007.03.008
[34] J.I. Escalante-Garcia, Nonevaporable water from neat OPC and replacement materials in composite cements hydrated at different temperatures, Cem Concr Res. 33 (2003) 1883-1888. https://doi.org/10.1016/S0008-8846(03)00208-4
[35] P. Mounanga, A. Khelidj, A. Loukili, V. Baroghel-Bouny, Predicting Ca(OH)2 content and chemical shrinkage of hydrating cement pastes using analytical approach, Cem Concr Res. 34 (2004) 255-265. https://doi.org/10.1016/j.cemconres.2003.07.006
[36] C. Gallé, Effect of drying on cement-based materials pore structure as identified by mercury intrusion porosimetry - A comparative study between oven-, vacuum-, and freeze-drying, Cem Concr Res. 31 (2001) 1467-1477. https://doi.org/10.1016/S0008-8846(01)00594-4
[37] J. Zhang, G.W. Scherer, Comparison of methods for arresting hydration of cement, Cem Concr Res. 41 (2011) 1024-1036. https://doi.org/10.1016/j.cemconres.2011.06.003
[38] D. Snoeck, L.F. Velasco, A. Mignon, S. Van Vlierberghe, P. Dubruel, P. Lodewyckx, N. De Belie, The influence of different drying techniques on the water sorption properties of cement-based materials, Cem Concr Res. 64 (2014) 54-62. https://doi.org/10.1016/j.cemconres.2014.06.009
[39] L. Zhang, F.P. Glasser, Critical examination of drying damage to cement pastes, Advances in Cement Research. 12 (2000) 79-88. https://doi.org/10.1680/adcr.2000.12.2.79
[40] J. Zhang, G.W. Scherer, Comparison of methods for arresting hydration of cement, Cem Concr Res. 41 (2011) 1024-1036. https://doi.org/10.1016/j.cemconres.2011.06.003
[41] A. Korpa, R. Trettin, The influence of different drying methods on cement paste microstructures as reflected by gas adsorption: Comparison between freeze-drying (F-drying), D-drying, P-drying and oven-drying methods, Cem Concr Res. 36 (2006) 634-649. https://doi.org/10.1016/j.cemconres.2005.11.021
[42] W. Deboucha, N. Leklou, A. Khelidj, M.N. Oudjit, Hydration development of mineral additives blended cement using thermogravimetric analysis (TGA): Methodology of calculating the degree of hydration, Constr Build Mater. 146 (2017) 687-701. https://doi.org/10.1016/j.conbuildmat.2017.04.132
[43] I. Pane, W. Hansen, Investigation of blended cement hydration by isothermal calorimetry and thermal analysis, Cem Concr Res. 35 (2005) 1155-1164. https://doi.org/10.1016/j.cemconres.2004.10.027
[44] C. Gosselin, K.L. Scrivener, Microstructure development of calcium aluminate cement accelerated with lithium sulphate, in: Calcium Aluminate Cements: Proceedings of the Centenary Conference, Avignon, June 30-July 2, 2008, 2008.
[45] L. Gomez-Zamorano, M. Balonis, B. Erdemli, N. Neithalath, G. Sant, C-(N)-S-H and N-A-S-H gels: Compositions and solubility data at 25°C and 50°C, Journal of the American Ceramic Society. 100 (2017) 2700-2711. https://doi.org/10.1111/jace.14715
[46] B. Walkley, X. Ke, O. Hussein, J.L. Provis, Thermodynamic properties of sodium aluminosilicate hydrate (N-A-S-H), Dalton Transactions. 50 (2021) 13968-13984. https://doi.org/10.1039/D1DT02202D
[47] B. Lothenbach, E. Bernard, U. Mäder, Zeolite formation in the presence of cement hydrates and albite, Physics and Chemistry of the Earth. 99 (2017) 77-94. https://doi.org/10.1016/j.pce.2017.02.006
[48] T. Williamson, L.E. Katz, J. Han, H.A. Dobbs, B.F. Chmelka, G. Sant, M.C.G. Juenger, Relationship between aqueous chemistry and composition, structure, and solubility of sodium aluminosilicate hydrates, Journal of the American Ceramic Society. 103 (2020) 2160-2172. https://doi.org/10.1111/jace.16868
[49] A. Mendoza-Flores, M. Villalobos, T. Pi-Puig, N.V. Martínez-Villegas, Revised aqueous solubility product constants and a simple laboratory synthesis of the Pb(II) hydroxycarbonates: Plumbonacrite and hydrocerussite, Geochem J. 51 (2017) 315-328. https://doi.org/10.2343/geochemj.2.0471
[50] B. Lothenbach, L. Pelletier-Chaignat, F. Winnefeld, Stability in the system CaO-Al2O3-H2O, Cem Concr Res. 42 (2012) 1621-1634. https://doi.org/10.1016/j.cemconres.2012.09.002
[51] L. Gomez-Zamorano, M. Balonis, B. Erdemli, N. Neithalath, G. Sant, C-(N)-S-H and N-A-S-H gels: Compositions and solubility data at 25°C and 50°C, Journal of the American Ceramic Society. 100 (2017) 2700-2711. https://doi.org/10.1111/jace.14715
[52] T. Wagner, D.A. Kulik, F.F. Hingerl, S. V. Dmytrievava, Gem-selektor geochemical modeling package: TSolMod library and data interface for multicomponent phase models, Can Mineral. 50 (2012) 1173-1195. https://doi.org/10.3749/canmin.50.5.1173
[53] Y. Xiong, Estimation of medium effects on equilibrium constants in moderate and high ionic strength solutions at elevated temperatures by using specific interaction theory (SIT): Interaction coefficients involving Cl, OH- and Ac- up to 200°C and 400 bars, Geochem Trans. 7 (2006) 1-19. https://doi.org/10.1186/1467-4866-7-4
[54] K.S. Pitzer, Characteristics of very concentrated aqueous solutions, Physics and Chemistry of the Earth. 13-14 (1981) 249-272. https://doi.org/10.1016/0079-1946(81)90013-6
[55] H.C. Helgeson, D.H. Kirkham, G.C. Flowers, Theoretical prediction of the thermodynamic behavior of aqueous electrolytes at high pressures and temperatures: IV. Calculation of activity coefficients, osmotic coefficients, and apparent molal and standard and relative partial molal properties to 600oC and 5 kb., Am J Sci. 281 (1981) 1249-1516. https://doi.org/10.2475/ajs.281.10.1249
[56] M. Ben Haha, G. Le Saout, F. Winnefeld, B. Lothenbach, Influence of activator type on hydration kinetics, hydrate assemblage and microstructural development of alkali activated blast-furnace slags, Cem Concr Res. 41 (2011) 301-310. https://doi.org/10.1016/j.cemconres.2010.11.016
[57] F. Puertas, S. Martínez-Ramírez, S. Alonso, T. Vázquez, Alkali-activated fly ash/slag cements. Strength behaviour and hydration products, Cem Concr Res. 30 (2000) 1625-1632. https://doi.org/10.1016/S0008-8846(00)00298-2
[58] T. Williamson, M.C.G. Juenger, The role of activating solution concentration on alkali-silica reaction in alkali-activated fly ash concrete, Cem Concr Res. 83 (2016) 124-130. https://doi.org/10.1016/j.cemconres.2016.02.008
[59] S. Alonso, A. Palomo, Calorimetric study of alkaline activation of calcium hydroxide-metakaolin solid mixtures, Cem Concr Res. 31 (2001) 25-30. https://doi.org/10.1016/S0008-8846(00)00435-X
[60] W. Rakngan, T. Williamson, R.D. Ferron, G. Sant, M.C.G. Juenger, Controlling workability in alkali-activated Class C fly ash, Constr Build Mater. 183 (2018) 226-233. https://doi.org/10.1016/j.conbuildmat.2018.06.174
[61] X. Guo, H. Shi, W.A. Dick, Compressive strength and microstructural characteristics of class C fly ash geopolymer, Cem Concr Compos. 32 (2010) 142-147. https://doi.org/10.1016/j.cemconcomp.2009.11.003
[62] D. Prentice, S. Bernal, M. Bankhead, M. Hayes, J. Provis, Using the Pitzer Model to Predict Aqueous Solution Compositions of Portland Cements Blended with Supplementary Cementitious Materials, in: Proceedings of International Conferences (ICACMS) Advances in Construction Materials and Systems Vol 2, RILEM Publications SARL, 2017, 638-647.
[63] M.U. Okoronkwo, M. Balonis, L. Katz, M. Juenger, G. Sant, A thermodynamics-based approach for examining the suitability of cementitious formulations for solidifying and stabilizing coal-combustion wastes, J Environ Manage. 217 (2018) 278-287. https://doi.org/10.1016/j.jenvman.2018.02.095

[64] D. Prentice, Thermodynamic modelling of ultra-long-term durability of cementitious binders for waste immobilisation, PhD Dissertation, The University of Sheffield, 2018.
[65] R.J. Myers, B. Lothenbach, S.A. Bernal, J.L. Provis, Thermodynamic modelling of alkali-activated slag cements, Applied Geochemistry. 61 (2015) 233-247. https://doi.org/10.1016/j.apgeochem.2015.06.006
[66] R.J. Myers, S.A. Bernal, J.L. Provis, A thermodynamic model for C-(N-)A-S-H gel: CNASH-ss. Derivation and validation, Cem Concr Res. 66 (2014) 27-47. https://doi.org/10.1016/j.cemconres.2014.07.005
[67] J. Ederová, V. Šatava, Heat capacities of C3AH6, C4AŠH12 and C6AŠ3H32, Thermochim Acta. 31 (1979) 126-128. https://doi.org/10.1016/0040-6031(79)80016-7
[68] C.A. Geiger, E. Dachs, A. Benisek, Thermodynamic behavior and properties of katoite (hydrogrossular): A calorimetric study, American Mineralogist. 97 (2012) 1252-1255. https://doi.org/10.2138/am.2012.4106
[69] P. Blanc, X. Bourbon, A. Lassin, E.C. Gaucher, Chemical model for cement-based materials: Thermodynamic data assessment for phases other than C-S-H, Cem Concr Res. 40 (2010) 1360-1374. https://doi.org/10.1016/j.cemconres.2010.04.003
[70] B. Ma, B. Lothenbach, Synthesis, characterization, and thermodynamic study of selected Na-based zeolites, Cem Concr Res. 135 (2020) 106111. https://doi.org/10.1016/j.cemconres.2020.106111
[71] M. Balonis, The influence of inorganic chemical accelerators and corrosion inhibitors on the mineralogy of hydrated Portland Cement Systems (PhD Dissertation), University of Aberdeen, Aberdeen, United Kingdom, 2010. https://doi.org/10.1016/j.cemconres.2010.03.002
[72] T. Thoenen, D. Kulik, Nagra/PSI Chemical Thermodynamic Data Base 01/01 for the GEM-Selektor (V.2-PSI) Geochemical Modeling Code: Release 28-02-03. Internal Report TM-44-03-04, 2003.
[73] T. Thoenen, W. Hummel, U. Berner, E. Curti, The PSI/Nagra Chemical Thermodynamic Database 12/07, PSI Report 14-04, Villigen PSI, Switzerland, 2014.
[74] T. Williamson, T. Zhu, J. Han, G. Sant, O.B. Isgor, L. Katz, M. Juenger, Effect of Temperature on N-A-S-(H) Composition, Solubility, and Structure, In Preparation. (n.d.).
[75] B. Ma, B. Lothenbach, Synthesis, characterization, and thermodynamic study of selected K-based zeolites, Cem Concr Res. 148 (2021). https://doi.org/10.1016/j.cemconres.2021.106537
[76] H.C. Helgeson, J.M. Delany, W.H. Nesbitt, D.K. Bird, Summary and critique of the thermodynamic properties of rock-forming minerals, Am J Sci. 278-A (1978) 1-229.
[77] D.A. Kulik, Thermodynamic properties of surface species at the mineral-water interface under hydrothermal conditions: A gibbs energy minimization single-site 2pK(A) triple-layer model of rutile in NaCl electrolyte to 250°C, Geochim Cosmochim Acta. 64 (2000) 3161-3179. https://doi.org/10.1016/S0016-7037(00)00413-0
[78] D.A. Kulik, Kulik, D. A. (2002). Minimising uncertainty induced by temperature extrapolations of thermodynamic data: a pragmatic view on the integration of thermodynamic databases into geochemical computer codes., in: The Use of Thermodynamic Databases in Performance Assessment, Barcelona, Spain, 2002: pp. 125-137.
[79] J. Shekhovtsova, I. Zhernovsky, M. Kovtun, N. Kozhukhova, I. Zhernovskaya, E. Kearsley, Estimation of fly ash reactivity for use in alkali-activated cements - A step towards sustainable building material and waste utilization, J Clean Prod. 178 (2018) 22-33. https://doi.org/10.1016/j.jclepro.2017.12.270
[80] M. Sadique, H. Al-Nageim, W. Atherton, L. Seton, N. Dempster, Mechano-chemical activation of high-Ca fly ash by cement free blending and gypsum aided grinding, Constr Build Mater. 43 (2013) 480-489. https://doi.org/10.1016/j.conbuildmat.2013.02.050
[81] R.F. Feldman, Helium flow and density measurement of the hydrated tricalcium silicate - water system, Cem Concr Res. 2 (1972) 123-136. https://doi.org/10.1016/0008-8846(72)90028-2
[82] M. Balonis, F.P. Glasser, The density of cement phases, Cem Concr Res. 39 (2009) 733-739. https://doi.org/10.1016/j.cemconres.2009.06.005
[83] I.G. Richardson, The calcium silicate hydrates, Cem Concr Res. 38 (2008) 137-158. https://doi.org/10.1016/j.cemconres.2007.11.005
[84] M. Balonis, B. Lothenbach, G. le Saout, F.P. Glasser, Impact of chloride on the mineralogy of hydrated Portland cement systems, Cem Concr Res. 40 (2010) 1009-1022. https://doi.org/10.1016/j.cemconres.2010.03.002
[85] F. Bellmann, J. Majzlan, K.D. Grevel, E. Dachs, H.M. Ludwig, Analysis of thermodynamic data of calcium aluminate monocarbonate hydrate, Cem Concr Res. 116 (2019) 89-94. https://doi.org/10.1016/j.cemconres.2018.10.012
[86] J.C. Lashley, M.F. Hundley, A. Migliori, J.L. Sarrao, P.G. Pagliuso, T.W. Darling, M. Jaime, J.C. Cooley, W.L. Hults, L. Morales, D.J. Thoma, J.L. Smith, J. Boerio-Goates, B.F. Woodfield, G.R. Stewart, R.A. Fisher, N.E. Phillips, Critical examination of heat capacity measurements made on a quantum design physical property measurement system, Cryogenics (Guildf). 43 (2003) 369-378. https://doi.org/10.1016/S0011-2275(03)00092-4
[87] Q. Shi, C.L. Snow, J. Boerio-Goates, B.F. Woodfield, Accurate heat capacity measurements on powdered samples using a Quantum Design physical property measurement system, Journal of Chemical Thermodynamics. 42 (2010) 1107-1115. https://doi.org/10.1016/j.jct.2010.04.008
[88] A. Jayalath, R. San Nicolas, M. Sofi, R. Shanks, T. Ngo, L. Aye, P. Mendis, Properties of cementitious mortar and concrete containing micro-encapsulated phase change materials, Constr Build Mater. 120 (2016) 408-417. https://doi.org/10.1016/j.conbuildmat.2016.05.116
[89] C.J.M. Houtepen, H.N. Stein, The enthalpies of formation and of dehydration of some AFm phases with singly charged anions, Cem Concr Res. 6 (1976) 651-658. https://doi.org/10.1016/0008-8846(76)90029-6
[90] H.A. Berman, E.S. Newman, Heat of formation of calcium aluminate monosulfate at 25 °C, J Res Natl Bur Stand A Phys Chem. 67A (1963) 1-13. https://doi.org/10.6028/jres.067A.001
[91] W. Yong, E. Dachs, A. Benisek, R.A. Secco, Heat capacity, entropy and phase equilibria of stishovite, Phys Chem Miner. 39 (2012) 153-162. https://doi.org/10.1007/s00269-011-0470-z
[92] J.J. Calvin, M. Asplund, Y. Zhang, B. Huang, B.F. Woodfield, Heat capacity and thermodynamic functions of γ-Al2O3, J Chem Thermodyn. 112 (2017) 77-85. https://doi.org/10.1016/j.jct.2017.04.011
[93] S. Ghazizadeh, T. Hanein, J.L. Provis, T. Matschei, Estimation of standard molar entropy of cement hydrates and clinker minerals, Cem Concr Res. 136 (2020) 106188. https://doi.org/10.1016/j.cemconres.2020.106188